

Kinetics of polymer looping with macromolecular crowding: effects of volume fraction and crowder size

Jaehoon Shin,¹ Andrey G. Cherstvy,¹ and Ralf Metzler^{1,2,*}

¹*Institute for Physics & Astronomy, University of Potsdam, D-14476 Potsdam-Golm, Germany*

²*Department of Physics, Tampere University of Technology, FI-33101 Tampere, Finland*

The looping of polymers such as DNA is a fundamental process in the molecular biology of living cells, whose interior is characterised by a high degree of molecular crowding. We here investigate in detail the looping dynamics of flexible polymer chains in the presence of different degrees of crowding. From the analysis of the looping-unlooping rates and the looping probabilities of the chain ends we show that the presence of small crowders typically slow down the chain dynamics but larger crowders may in fact facilitate the looping. We rationalise these non-trivial and often counterintuitive effects of the crowder size onto the looping kinetics in terms of an effective solution viscosity and standard excluded volume effects. Thus for small crowders the effect of an increased viscosity dominates, while for big crowders we argue that confinement effects (caging) prevail. The tradeoff between both trends can thus result in the impediment or facilitation of polymer looping, depending on the crowder size. We also examine how the crowding volume fraction, chain length, and the attraction strength of the contact groups of the polymer chain affect the looping kinetics and hairpin formation dynamics. Our results are relevant for DNA looping in the absence and presence of protein mediation, DNA hairpin formation, RNA folding, and the folding of polypeptide chains under biologically relevant high-crowding conditions.

Abbreviations: MMC, macromolecular crowding; PDF, probability density function; LJ, Lennard-Jones; FENE, finitely-extensible non-linear elastic; PEG, polyethelene glycol; ssDNA, single-stranded DNA; ds-DNA, double-stranded DNA; MW, molecular weight; MSD, mean squared displacement.

I. INTRODUCTION

Molecular reactions in living biological cells are running off in a highly complex environment, that is compartmentalised by membrane structures and crowded with macromolecules and structural cytoskeletal networks. Macromolecular crowding (MMC) makes up a “superdense”¹ environment modulating the kinetics of various biochemical processes in cells. Inter alia, this mechanism is employed biologically to tune the DNA accessibility in the cyto- and nucleoplasm. MMC non trivially influences the levels of gene expression, and the size of the crowders dramatically modifies the response of genetic elements². In particular, it was found that in solutions of small crowders the rate of gene expression only varies slightly with the volume fraction ϕ of the crowders, while large crowders boost the expression levels many-fold².

More specifically, MMC constitutes a non-specific environment controlling the looping properties of biopolymers such as nucleic acids and polypeptides. Polymer looping is indeed a ubiquitous mechanism of DNA protection, compaction, and gene regulation in both bacteria and higher organisms³. DNA looping is vital for the regulation of transcription and effects the robustness of bio-switches⁴. The effects of MMC on kinetics of DNA looping are of paramount importance for the speed, efficiency, and precision of gene regulatory networks^{2,5,6}.

Inspired by the impressive body of experimental evidence for the relevance of MMC on biochemical processes, we here scrutinise the key role of the crowder size for the kinetics and thermodynamics of polymer looping.

The quantitative study of the diffusion-limited encounter of the end monomers of a polymer chain in a mixture of crowders of varying sizes and the analysis of the effective viscosity of the solution is a formidable theoretical problem. Despite the progress of the understanding of polymer looping and cyclisation at dilute solvent conditions by theoretical approaches^{7–10} and by simulations^{11–17}, polymer looping in the presence of MMC^{18–20} still poses a number of challenges, which are our main targets here.

It is known that MMC generally facilitates the association of proteins via volume exclusion effects and favours more compact states²¹. Polymer looping, however, involves the diffusion of an extended and chain length-dependent fragment of the polymer in crowded solutions. This non-locality effect renders the trends of the inhibition or facilitation of polymer looping kinetics in the presence of MMC less intuitive. Looping is a fundamental dynamic property of polymers which can be directly probed by methods such as fluorescence energy transfer²². A comprehensive theory of polymer looping under crowded conditions is not straightforward. We here employ extensive crowder-explicit simulations of polymer looping including a number of important physical and biochemical ingredients.

Polymer organisation in the presence of MMC and spatial confinement is a common theme in biophysics²³. It affects, for instance, the segregation of DNA rings in dividing bacteria cells^{24,25} as well as the territorial organisation of DNA inside eukaryotic nuclei²⁶ and bacteria²⁷. Of particular interest is polymer looping and knotting in MMC-dominated solvents^{28–30}. The highly crowded

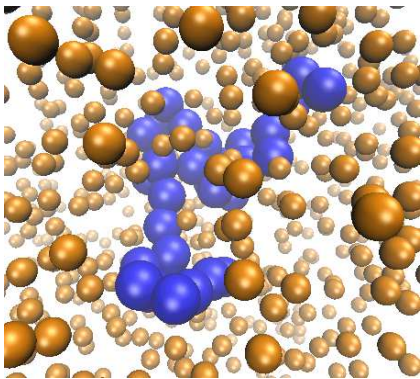


FIG. 1: Typical polymer conformation in the presence of MMC. The polymer chain (blue spheres) consists of $n = 32$ monomers, the fraction of crowders (golden spheres, rendered smaller for better visibility of the polymer) is $\phi = 0.1$, and the size of the crowders is $d_{cr} = 1\sigma$ in terms of the monomer diameter σ of the polymer chain. Video-files illustrating the dynamics looping dynamics of polymer chains for small and big crowders are included in the Supporting Information.

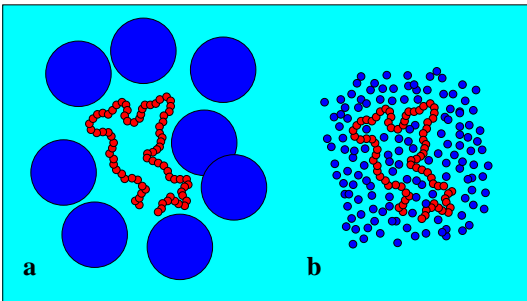


FIG. 2: Crowder size effect: Large crowders lead to the caging of the polymer (a), while small crowders tend to mix with the chain monomers (b) and increase the effective viscosity. Note that the size of the chain is the same in both images.

environments of real biological cells feature volume occupancies of up to $\phi \sim 30\%$ ^{31,32}. In vitro, concentrated solutions of naturally occurring proteins, globular and branched polymers (lysozyme, serum albumin, PEG, dextran, Ficoll, etc.) mimic MMC conditions in a more controlled environment^{33,34}. On top of MMC volume exclusion, the eukaryotic cytoskeleton forms a spatial mesh with a period of several tens of nm affecting the diffusion of cellular components.

Excluded-volume interactions by crowders favour molecular association reactions³⁵, speed up the folding of proteins into their native structures³⁶⁻⁴⁰, and facilitate the assembly of virus capsids⁴¹. The effects of the crowder size were studied for polypeptide folding⁴² and protein fibrillation³⁵. We note that apart from MMC in the cytosol of biological cells, crowding is also an important ingredient for the diffusional dynamics of embedded proteins and lipid molecules in biological membranes⁴³⁻⁴⁵.

Also note that the thermodynamics and the demixing transitions in the mixtures of colloidal particles and linear polymers have been explored⁴⁷, in particular in the limit of long polymers (the so-called "protein limit")⁴⁶.

The biological relevance for the study of polymer looping is due to its central role in gene regulation, for instance, in the formation of DNA loops induced by transcription factor proteins such as Lac or λ repressor⁴⁸⁻⁵⁰. Inter-segmental protein jumps along DNA made possible via looping facilitate protein diffusion in DNA coils^{51,52} and affects MMC-mediated gene regulation^{2,5,53,54}. Another example is the dynamics of the DNA chain itself on various levels of DNA structural organisation ranging from the bare DNA, via chromatin fibres, to complex chromosomal filaments^{3,55}. We also mention protein-⁵⁶ and RNA-folding⁵⁷ reactions.

Experimentally, the effects of polymeric crowders onto the opening-closing dynamics of ssDNA hairpins with complementary sticky ends^{58,59} were studied in detail⁶⁰. It was demonstrated in Ref.⁶⁰ that ssDNA hairpin formation dynamics is dramatically slowed down in highly-crowded solutions of dextran and PEG of varying molecular weights (MWs), $MW \sim 0.2-10$ kDa. Also, the fraction of open hairpins gets reduced substantially by relatively large crowders, in contrast to low-MW solutions of sucrose. In the latter, the similarly slowed-down DNA hairpin dynamics due to a higher viscosity of the medium, the fraction of hairpins stayed nearly constant with crowding. Note that the experimental setup of Ref.⁶⁰ only allowed to measure the geometric average of looping-unlooping times τ_K . A separate measurement of looping T_l and unlooping T_{ul} times of the cohesive chain ends as a function of MMC fraction ϕ was not feasible. The fraction of time the hairpins are in a looped state was also measured⁶⁰.

Some effects of MMC on polymer looping were analysed recently^{11,19}. For instance, for *implicit* attractive depletion potentials between polymer segments (mimicking MMC) the polymer looping (T_l) and unlooping (T_{ul}) times (see below) for $\phi = 0.15$ and fixed size of crowders were quantified by simulations¹¹. For long chains, the increase of the looping time T_l obeys the scaling relation

$$T_l(n) \sim n^{2\nu+1} \sim n^{2.2} \quad (1)$$

with the chain length $l = n\sigma$ ¹¹. Here $\nu \approx 3/5$ is the Flory exponent⁹⁰. Relation (1) is indeed supported by polymer cyclisation theory¹⁶. Experimentally, the rate of formation of DNA hairpins drops somewhat faster with the chain length, $T_l(n) \sim n^{2.6 \pm 0.3}$, probably due to excluded-volume effects⁵⁸. Moreover, it was predicted that due to a non-trivial interplay of the enhanced solution viscosity and polymer "crumpling" the looping time varies non-monotonically with ϕ ¹¹.

In contrast, the unlooping time T_{ul} exhibits only a weak dependence on the chain length¹¹. A finite cohesive energy of polymer ends, $\epsilon_s > 0$, gives rise to more extended "looped" periods and longer unlooping times¹¹. The looping time, the time separating the extended and looped states of the chain, becomes shorter

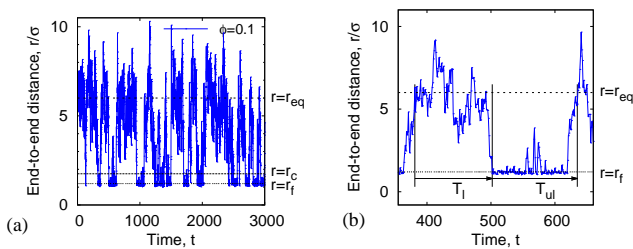


FIG. 3: Time evolution of the polymer end-to-end distance and definition of the looping-unlooping $T_{l,ul}$ and opening-closing $T_{op,cl}$. The equilibrium r_{eq} and critical r_c distances are indicated. The simulated chain consists of $n = 16$ monomers, and the crowding fraction is $\phi = 0.1$.

due to “depletion-based crowding” for longer chains, i.e., more compact polymer states are favoured, effecting a slow-down of the unlooping dynamics¹¹.

We here report results from extensive Langevin dynamics simulations of the looping of Rouse-like flexible polymers in solutions of *explicit* nearly hard-sphere crowders (see Fig. 1). We examine the effects of the crowding volume fraction ϕ , the crowder diameter d_{cr} , the stickiness ϵ_s of the end monomers, and the chain length $n\sigma$, where σ is the monomer diameter. We showed recently²⁵ that for two polymer *rings* under confinement and crowding conditions the contact properties are non-monotonic in the crowding fraction ϕ . Here, we demonstrate that MMC has unexpected effects on the looping dynamics as well, due to competition between depletion effects facilitating looping and an increased effective solution viscosity slowing down the looping kinetics, see Figs. 1, 2.

II. MODEL AND METHODS

To study polymer-nanoparticle mixtures by computer simulations, Monte-Carlo and Molecular Dynamics investigations were conducted in the literature to elucidate the static and dynamical behaviour of binary mixtures of polymers and crowders. Important ingredients were included in simulations to render the results applicable to realistic situations, for instance, in cells. Thus, the effects of compressible polymers⁶¹, non-spherical⁶² and charged crowding nanoparticles^{63,64} onto polymer-crowder demixing as well as the implications of confinement^{65,66} and viscoelastic effects⁶⁸ on polymer looping kinetics were studied.

Computer simulations¹¹ revealed e.g. that the unlooping time T_{ul} stays nearly constant with n and increases 3-4 times as crowding fraction grows from $\phi = 0$ to 0.15. Note that because of a limited applicability of the effective depletion potentials used, only moderate ϕ values were studied in Ref.¹¹. The unlooping time T_{ul} is defined in our study as the time required for the chain to expand from the close-end to the equilibrium state, somewhat different from the definition used in Ref.¹¹, see Fig. 3.

A. Potentials and Approximations

Performing Langevin dynamics simulations of flexible polymers, we here examine the looping probabilities of the chain ends in the presence of MMC. The polymer chain is modelled within bead-spring model with finitely extensible nonlinear elastic (FENE) potentials,

$$U_{\text{FENE}}(r) = -\frac{k}{2}r_{\text{max}}^2 \log\left(1 - \frac{r^2}{r_{\text{max}}^2}\right). \quad (2)$$

Here k is the spring constant and r_{max} is the maximum allowed separation between the neighbouring polymer monomers. Excluded-volume interactions between polymer segments are given by the standard truncated Lennard-Jones (LJ) repulsive potential (Weeks-Chandler-Andersen potential),

$$U_{\text{LJ}}(r, \epsilon) = \begin{cases} 4\epsilon[(\sigma/r)^{12} - (\sigma/r)^6] + \epsilon, & r < r_{\text{cutoff}} \\ 0, & \text{otherwise} \end{cases} \quad (3)$$

with $r_{\text{cutoff}} = 2^{1/6}\sigma$. Here, r is the monomer-monomer distance, σ is the chain monomer diameter, and ϵ is the strength of the potential. We set $k = 30$, $r_{\text{max}} = 1.5$ (to minimise bond crossings⁶⁷ of the chain), and $\epsilon = 1$ (with all the energies being measured in units of the thermal energy, $k_B T$). Similar repulsive 6-12 LJ potentials parameterise the (chain monomer)-crowder and crowder-crowder interactions.

The chain monomer diameter is set in simulations to $\sigma = 4$ nm, determining polymer thickness and its effective viscosity in the crowded solution, η . The diameter d_{cr} of mono-disperse hard-core repulsive crowding particles varies in simulations in the range $0.75 \leq d_{cr} \leq 8\sigma$. The mass density is kept constant for all crowder sizes, fixed to the value known for average cytoplasm-crowding macromolecules¹⁸. Thus, for the varying crowder sizes its mass grows as $m_{cr} \sim d_{cr}^3$ and the friction coefficient increases according to the “effective” Stokes-Einstein law as $\xi_{cr} \sim d_{cr}$, similar to the procedure of Ref.⁷⁶. We use a cubic simulation box with volume $V = L^3$ and periodic boundary conditions. The volume fraction of crowders is $\phi = N_{cr}V_{cr}/V$, where N_{cr} is the number of crowders and $V_{cr} = \frac{4}{3}\pi(d_{cr}/2)^3$ the volume of each crowding particle. The characteristic time scale for a crowder with $d_{cr} = 1\sigma$ and $m_{cr} = 67.7$ kDa¹⁸ is $\delta\tau = d_{cr}\sqrt{m_{cr}/(k_B T)} \approx 0.36$ ns. The times presented in the figures below are in the units of this elementary time step $\delta\tau$. The features of the crowder size we observe with this explicit simulation scheme would not be visible in more coarse-grained models of crowded media employed previously, including those with effective depletion potentials.

The dynamics of position $\mathbf{r}_i(t)$ of the chain monomers

is described by the Langevin equation

$$m \frac{d^2 \mathbf{r}_i(t)}{dt^2} = - \sum_{j=1, j \neq i}^N \nabla U_{\text{LJ}}(|\mathbf{r}_i - \mathbf{r}_j|) - \nabla U_{\text{FENE}}(|\mathbf{r}_i - \mathbf{r}_{i \pm 1}|) - \sum_{j=1}^{N_{\text{cr}}} \nabla U_{\text{LJ}}(|\mathbf{r}_i - \mathbf{r}_{\text{cr},j}|) - \xi \mathbf{v}_i(t) + \mathbf{F}_i(t). \quad (4)$$

Here m is the mass of the monomer, ξ is the monomer friction coefficient and $\mathbf{F}_i(t)$ is the white Gaussian noise with the correlator $\langle \mathbf{F}_i(t) \cdot \mathbf{F}_j(t') \rangle = 6\xi k_B T \delta_{ij} \delta(t - t')$ that couples the particle friction and diffusivity $D = k_B T / \xi$. Similarly to the procedure described in Ref.⁶⁹, we implement the velocity Verlet algorithm with the integration time step of $0.002 \leq \Delta t \leq 0.01$. Smaller simulation step was used for bigger crowders and higher volume fractions ϕ .

The terminal monomers interact with the energy ϵ_s which mimics e.g. the energetic profit for the formation of closed ssDNA hairpin structures via hydrogen-bonding pairing interactions between the complementary bases on the end DNA fragments. Although we simulate flexible polymers, via corresponding rescaling the effective monomer size, the results can be applicable to looping of semi-flexible dsDNA as well, where the loop/ring joining reaction is often supported by the ligation enzymes^{70,71}. The number of the chain monomers n vary in simulations in the range $10 \leq n \leq 256$. The pairing energy of $\epsilon_s = 5k_B T$ used in the majority of results below can be considered as a good estimate for pairing propensity in DNA hairpins with not too long complementary ends, see Ref.⁶⁰. We examine the range of chain end cohesiveness of $0 \leq \epsilon_s \leq 10k_B T$.

We simulate the attractive end-to-end interactions via the same LJ potential, Eq. (3), but with larger cutoff distance and bond intensity ϵ_s , namely $U_{\text{attr}}(r) = U_{\text{LJ}}(r, \epsilon_s) + C_{\text{LJ}}$ and $r_{\text{cutoff}} = 3\sigma$. Along with this longer cutoff distance we shift the entire LJ potential in the vertical direction by the constant C_{LJ} so that at $r = r_{\text{cutoff}}$ the potential becomes continuous with the zero-value branch at larger distances $r > r_{\text{cutoff}}$. The volume fraction of mono-disperse crowders is varied in our simulations up to $\phi = 0.3$; see Ref.⁷² for even denser colloidal systems.

The free energy of ssDNA hairpin formation contains two contributions: the favourable stacking/pairing of the helical dsDNA part and the entropic penalty of the looped part. The sum of the two for real DNAs is a complicated function of DNA sequence and other model parameters^{73,75} amounting to ~ -2.1 kcal/mol $\approx -3.5 k_B T$ for about 20 bp long DNA hairpins used in Ref.⁶⁰. Longer complementary paired stem parts result in more stable hairpins, we mimic in simulations via larger values of end-to-end cohesive energy ϵ_s .

We neglect long-range interactions between polymer segments, including the electrostatic forces, that is a rea-

sonable approximation for long chains at physiological salt concentrations. In low-salt solutions, however, in application to DNA, the charge-charge electrostatic interactions will become important for the loop-closure probability and dynamics⁷⁷. We assume polymer-solvent interactions stays unaltered at increasing volume occupancies by crowders (see Ref.⁷⁸ for possible effects of MMC onto the properties of nucleic acid solutions at reduced solvent activity).

The hydrodynamic interactions are also neglected below (the Rouse polymer model), see Refs.⁷⁹⁻⁸¹ for some implications. The effects of hydrodynamic interactions onto end-monomers dynamics of dsDNA has been studied by fluorescence correlation spectroscopy experimentally in Refs.^{82,83}. Theoretically, the Rouse versus Zimm chain dynamics has been examined for semi-flexible polymers in solutions^{84,85}, confined spaces⁸⁶, and near surfaces⁸⁷. In the latter situation e.g. it was clearly demonstrated, based on the hydrodynamic Brownian simulations and the mean-field hydrodynamic theory, how the Zimm dynamics turns into the Rouse one as the polymer chain approaches the no-slip surface⁸⁷. In particular, for the end-to-end distance of the chain near the interface, the influence of hydrodynamic interactions screened as $\propto 1/r$ with the inter-particle distance, was shown to be marginal.¹¹⁴

B. Parameters and Data Analysis

We compute the end-joining statistics from the time series of the polymer end-to-end distance generated in simulations as follows. For looping, we start with the most probable end-to-end chain extension (the minimum of the free energy $F(r)$, see Eq. (5) and Fig. 4 below, $r = r_{\text{eq}}$) and let the chain ends diffuse to the final extension $r = r_f \approx 1.2\sigma$. (The contact distance between the terminal chain beads in the folded state implemented in Ref.¹¹ was somewhat different, $r_f = \sigma + d_{\text{cr}}$.) The looped state distance r_f corresponds to the minimum of the LJ potential in Eq. (3) and stays nearly constant in the whole range of model parameters used here.

The time required for the chain to join its ends is defined as the looping time T_l , see Fig. 3. The unlooping time T_{ul} is defined as the time required for the chain to expand back, from the jointed-ends state with $r = r_f$ to the equilibrium state at $r = r_{\text{eq}}$. This distance is a function of all model parameters, in particular of the chain length $l = n\sigma$ and the MMC fraction, that is accounted for in simulations below. The closing time T_{cl} is defined as the average time the polymer needs to diffuse from the last moment its end-to-end extension was $r = r_{\text{eq}}$ to the first moment with the close-contact distance of $r \approx r_f$. The opening time T_{op} is the minimal time for the chain ends to diffuse from the closed state $r = r_f$ to a first state with $r = r_{\text{eq}}$. In Fig. 3 we illustrate on a real end-to-end diffusion trace the definitions of the looping/unlooping and opening/closing times.

Likewise, the critical distance of $r_c = 1.75\sigma$ used below to define the occurrence of end-monomer contacts stays nearly constant. It approximately denotes the end-monomer separation at which the free energy barrier emerges which separates the close-looped and equilibrium states of the polymer, see Fig. 4 below. This critical distance r_c is used below to compute the looping probability P_l . One can think of other choices for r_c to mimic somewhat longer-ranged nature of end-end contacts.¹¹⁵

We study the end-to-end joining statistics; the implications of MMC onto looping kinetics of inner polymer monomers is beyond the scope of this study and will be presented elsewhere. The simulation time for the chains of $n=8, 32,$ and 128 monomers on a standard 3-3.5 GHz core machine is about 3, 4, and 60 h, respectively. The typical number of the looping events used for averaging procedure for these chain lengths is about 2000, 500, and 200, correspondingly. In some cases we use traces, that are twice as long, for a better statistics. The number of crowding molecules of size $d_{cr} = 1\sigma$ in the simulation box used to perform simulations of the polymer chains of these lengths is $N_{cr} \approx 1000, 3000,$ and 10000 , respectively. Moreover, we remark that instead of averaging over the ensemble of initial chain configurations, we rather analyse the individual simulated time traces of the end-to-end distance $r(t)$ to compute the chain looping characteristics.

We analysed the $r(t)$ data obtained from either single or multiple simulation runs, depending on the total computation time used. The typical running time, $t \sim 10^{5 \dots 7} \times \delta\tau$, is chosen much longer than all the time scales in the system, in order to avoid a bias in sampling of end-joining events. To perform the error analysis, we use different methods for the dynamic and static quantities. As looping events are rare, the time intervals between them are of the order of the chain relaxation time, and the events can be considered independent. Thus, we use the standard error of the mean to compute the error bars for the looping (unlooping) and opening (closing) times. For the static quantities, such as the radius of gyration of the polymer, we split the entire trajectory into ten sub-series, calculate the values for each of them, and then compute the standard deviations of those pre-averaged values to get the final error bar. Previously²⁵ we also used the so-called "blocking method" for the error analysis in correlated sets of data. Here we compare the two methods for a number of quantities and the differences in the sizes of the error bar were $\lesssim 30\%$.

We need to distinguish the MMC effects for small ($d_{cr} \ll R_g = \sqrt{\langle R_g^2 \rangle}$) and large crowders ($d_{cr} \gtrsim R_g$). Large crowders creates voids/cages between themselves which facilitate compaction of relatively short polymers and facilitate looping. The reader is referred to Sec. III G for the quantitative analysis of caging effects in our polymer-crowder mixtures. For longer chains, which do not fit into a single cavity and need to occupy the neighbouring voids, the effect of crowders on looping proba-

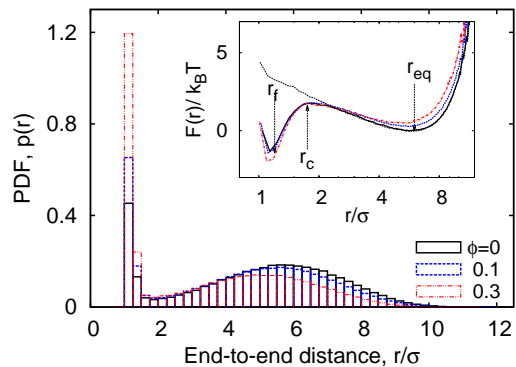


FIG. 4: Bimodal distribution $p(r)$ of the polymer end-to-end distance at varying MMC fraction ϕ . The inset is the free energy profile for looping, $F(r)$, with the most likely separation between the polymer ends shown as r_{eq} . The free energy profile for purely repulsive end monomers ($\epsilon_s = 0, \phi = 0$) is also shown as the dotted curve in the inset. Parameters: $\epsilon_s = 5k_B T, n = 16, d_{cr} = 1\sigma$.

bility can be *inverted*. A similar effect occurs in MMC-mediated protein folding, when small crowders favour the compact state of a protein, while larger ones can promote protein unfolding⁸⁸. The systematic investigation of crowder surface properties is the subject of our future investigations⁸⁹.

III. RESULTS: CROWDING AND POLYMER DYNAMICS

The equilibrium statistical behaviour of a linear flexible polymers with sticky ends is governed by the tradeoff between the enthalpically favourable pairing of the sticky ends and the entropy loss in the more compact looped state. In what follows we first rationalise the effects of MMC on the static properties of polymer looping. We then examine the kinetics of loop closure and opening as functions of the details of the crowders such as crowding fraction and crowder size.

A. Distribution Function $p(r)$ and Free Energy

Our simulations generate time traces of the end-to-end distance $r(t)$ between the two extremities of the linear polymer. These two end monomers interact through an attractive LJ potential with an attractive cohesiveness ϵ_s which is varied in the range $0 \leq \epsilon_s \leq 10k_B T$, see the specification of the system in the preceding section. The recorded dynamics for $r(t)$ exhibits the highly erratic dynamics shown in Fig. 3, see below for the exact definition of the looping and unlooping times. We first focus on the one-dimensional probability density function (PDF) $p(r)$ of the end-to-end distance, as shown in Fig. 4.

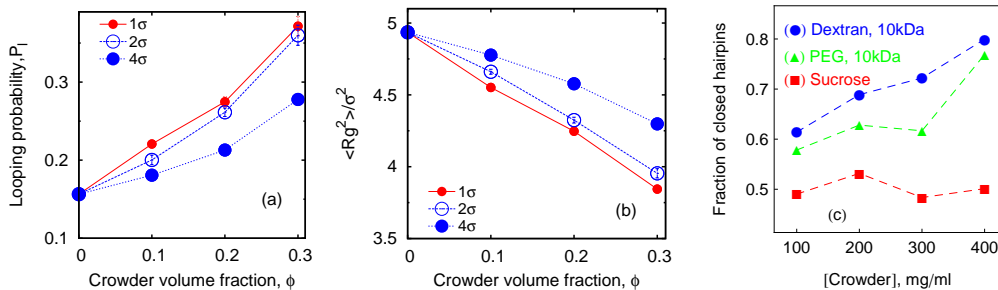


FIG. 5: Looping probability $P_l(\phi)$ (panel a) and polymer radius of gyration $R_g(\phi)$ (panel b) computed from simulations for $\epsilon_s = 5k_B T$, $n = 16$. Experimental data⁶⁰ for the fraction of closed ssDNA hairpins is shown in panel (c). Here and below the simulation data for $d_{cr} = 1 \times \sigma$ are presented as small red circles, big blue circles correspond to $d_{cr} = 4 \times \sigma$. Note that the weaker effect of larger ($d_{cr} = 4 \times \sigma$) crowders onto the dimensions of the polymer coil shown in panel (b) may be due to the matching of sizes ($R_g \sim d_{cr}$) for the relatively short chains considered here.

The relative motion of terminal monomers is subject to the free energy potential $F(r)$ that can be obtained from the PDF of the end-to-end distance $p(r)$ (see Fig. 4) via the inverse Boltzmann relation as

$$F(r) = -k_B T \log[p(r)]. \quad (5)$$

The presence of sticky chain ends gives rise to the formation of a double-well potential for $F(r)$, see Figs. 4 and A.1. The shallow free energy well related to the maximum of the PDF $p(r)$ corresponds to the equilibrium end-to-end chain distance in the absence of sticky ends, namely $r = r_{eq}$. This minimum is accompanied by a sharp free energy well at very close end-to-end distances due to the presence of sticky ends. The transition between the looped and unlooped states of the polymer takes place in this asymmetric $F(r)$ potential. The chain should overcome free energy barriers in the course of looping and unlooping. Simultaneously, the equilibrium chain extension $r_{eq}(n)$ is a growing function of the chain length, see Fig. A.1.¹¹⁶

B. Looping probability and polymer size

From $p(r)$ —which is a function of the number of monomers n —we compute the probability distribution

$$P_l = \int_{\sigma}^{r_c} p(r) dr \quad (6)$$

for the chain to be in the looped state as function of n , see Fig. A.1. That is, P_l is proportional to the number of configurations in which the sticky ends of the chain are within a maximum distance of $r_c = 1.75\sigma$. The lower cut-off discards thermodynamically unfavourable, rare events when the end beads are closer than the distance σ . For a single trajectory $r(t)$ of the end-to-end distance shown in Fig. 3, the probability $P_l(n)$ is then equal to the fraction of time during which the chain is looped.

Fig. 5a demonstrates that the looping probability P_l grows with the crowding fraction ϕ . This is in accord with recent results of ssRNA tertiary folding-unfolding dynamics⁵⁷ as well as ssDNA hairpin formation measurements⁶⁰ in crowded polymeric solutions. In the latter experiment, fluorescence correlation spectroscopy data indicated a linear increase of the fraction of closed ssDNA hairpins as function of ϕ ,

$$P_l(\phi) \sim A + B\phi, \quad (7)$$

see Fig. 5c. Our results reported here demonstrate that this trend becomes amplified for growing length $n\sigma$ of the polymer, as demonstrated in Fig. 6a. The magnitude of the relative facilitation for the looping probability for $\phi \approx 0.2$ is of the order of 2 to 4, compared with the dynamics in the absence of crowders. This value is similar to the experimental trends for ssDNA hairpin formation with MMC⁶⁰, compare Fig. 5c. This P_l -enhancement effect is present for both small and large crowders, as shown in Fig. 6a.

Consider now the PDF $p(r)$ shown in Fig. 4. It has a bimodal structure, reflecting the proximity between the sticky ends with end-to-end distances $r \approx \sigma$ and a broad distribution of r values reflecting the diffusive nature of the chains ends in the extended state. As can be seen in Fig. 4, the presence of MMC favours more compact polymer states: with increasing crowding fraction ϕ the polymer radius of gyration R_g decreases, in accord with common MMC effects^{21,56}. The significant shift of the distribution to shorter r values is particularly visible when the peak around $r \approx \sigma$ is considered.

For completeness we mention that, as expected a priori, stronger cohesiveness of the sticky ends favours higher looping probabilities P_l , reaching unity at $\epsilon_s \gg 1k_B T$ (see Fig. A.2) and yields progressively longer unlooping times. This fact also agrees with the experimental data on ssDNA hairpin formation in solutions of polymeric crowders of different MWs shown in Fig. 8. Interestingly, we find that for crowder molecules with larger

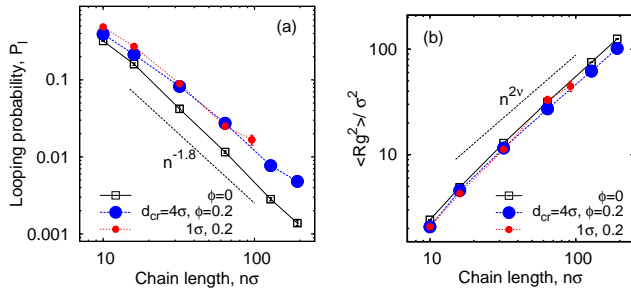


FIG. 6: Looping probability P_l and the gyration radius R_g versus the degree of polymerisation n . The asymptotes $P_l(n) \sim n^{-1.8}$ and $\langle R_g^2(n) \rangle \sim n^{2\nu}$ correspond to the dashed lines. Parameters: $\epsilon_s = 5k_B T$ and $\phi = 0, 0.2$. The crowder sizes are as indicated.

diameter d_{cr} the looping probability P_l becomes less sensitive to ϕ , as demonstrated in Fig. 5a (smaller values of B in Eq. (7)). To map the detailed parametric dependence of the looping statistics as function of chain length n , crowder size d_{cr} , and fraction ϕ is a major challenge for simulations. We examine all these effects below.

As shown in Fig. 6 for both small and large crowders the looping probability P_l decreases with the chain length n as

$$P_l(n) \sim n^{-1.8}. \quad (8)$$

The scaling exponent 1.8 law is close to the one of the Stockmayer formula $P_l(n) \simeq n^{-3\nu}$ for the looping of a self-avoiding polymer, where $3\nu \approx 1.76^{90}$. At the same time the radius of gyration of the chain grows as $\langle R_g^2(n) \rangle \simeq n^{2\nu}$, as expected for a self-avoiding chain⁹⁰. These dependencies are seen to be quite generic for varying crowder sizes d_{cr} and fractions ϕ , see Fig. 6.

The simulations yield instructive shapes for the polymer free energy $F(r) = -k_B T \log[p(r)]$ as shown in the insets of Fig. 4 and in Fig. A.1. We find a clear trend for the free energy barriers $\Delta F(n)$: for the transition from the unlooped to the looped state the barriers become higher for longer chains, as shown in Fig. A.1. This effect is due to the higher entropic penalty upon looping for longer polymers. In contrast, the barriers for a transition from the looped to the unlooped state are fairly insensitive to n , reflecting that unlooping is a *local activation* effect of dissolving the bond between the terminal monomers. This important feature gives rise to a more pronounced chain-length effect on the looping time T_l as compared to the analogous dependence of the unlooping time T_{ul} , as seen in Fig. 7. We now study the (un)looping times in more detail.

C. Looping and unlooping times

Fig. 3 shows how we extract the average looping and unlooping times T_l and T_{ul} from the time series $r(t)$ of the end-to-end distance. Namely, T_l is counted from

the point when—after a previous looped state—the chain ends reach their equilibrium distance r_{eq} until they touch close to the minimum of the attractive LJ potential. By definition, the equilibrium distance r_{eq} corresponds to the free energy minimum for the extended chain conformations. From that moment, T_{ul} is counted until the chain ends are separated by the distance r_{eq} again. The computation of T_l thus involves extensive chain rearrangements and thus non-trivially depends on the crowder fraction ϕ , which favours more compact states. In our analysis T_l and T_{ul} are then averaged over many looping events, the results being shown in Fig. A.3 for a fixed chain length.

The distribution of looping times is found to be nearly exponential, and the characteristic time is shorter in more crowded solutions of bigger crowders, see Fig. A.4. The full statistics and fluctuations of T_l can be envisaged from the PDFs presented in Fig. A.4. We fitted the $p(T_l)$ functions by two-parametric Weibull distributions of the form

$$p(T_l) \sim T_l^{\gamma-1} \exp[-(T_l/T_l^*)^\gamma]. \quad (9)$$

We found that the looping times are nearly exponentially distributed, with the parameter $1 \lesssim \gamma \lesssim 1.17$ being quite close to unity for all ϕ fractions and crowder sizes examined in Fig. A.4. Note that the nearly—but not exactly—exponential distribution $p(T_l)$ is indicative of some short-living ”intermediates” in the looping process. Note also that the first-encounter kinetics of the polymer ends is reminiscent of the first-passage kinetics of reactants in generalised biochemical networks, see e.g. Refs.^{91,92}. The decay length T_l^* of $p(T_l)$ distributions appears to be growing with ϕ for small crowders, while the decay of $p(T_l)$ gets faster with ϕ for larger crowders, see Fig. A.4 for $d_{cr} = 1\sigma$ and 4σ . This behaviour is physically consistent with the more restricted motions of the whole polymer and its ends at higher MMC fractions of bigger obstacles: the looping kinetics becomes faster and the spread of looping times gets narrower (more reliable looping events).

We also consider the opening and closing times T_{op} and T_{cl} (Fig. 3). T_{op} is the time for the chain ends to open up from a closed state and first reach the equilibrium distance r_{eq} . T_{cl} measures the time from the last occurrence of r_{eq} before a new looping event with $r < r_c$. Both T_{op} and T_{cl} grow with ϕ , as shown in Fig. A.5. These times are, as expected, much shorter than the looping and unlooping times. For T_{op} and T_{cl} we detect no significant difference in their ϕ dependence, consistent with theoretical⁹³ and experimental⁹⁴ results.

So what about the dependence on the crowder size? Fig. 7 demonstrates that for small crowders the looping kinetics is somewhat inhibited and T_l increases with ϕ . For large crowders, however, we observe the opposite and stronger trend: polymer looping is facilitated. As detailed in Fig. A.3a, T_l indeed decreases with ϕ up to $d_{cr} = 4\sigma$, however, for even larger crowders it starts to increase again, see Fig. A.3b. For very large crowders T_l

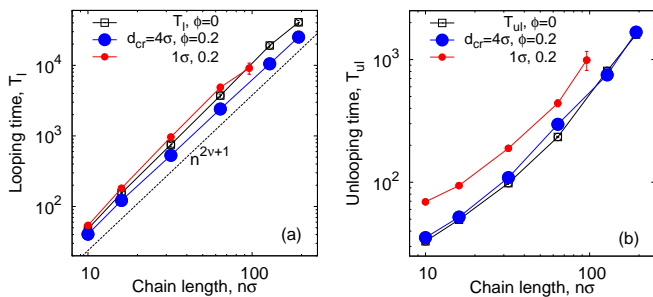


FIG. 7: Average looping (panel a) and unlooping (panel b) times versus the chain length. The asymptote (1) of $T_l(n) \sim n^{2\nu+1}$ in absence of crowders is shown by the dashed line in panel (a). Parameters are the same as in Fig. 6. The shown error bars are often smaller than the symbol size.

appears to approach the looping time in absence of crowders, indicated by the dashed line in Fig. A.3b. Fig. A.6 reveals that the solution viscosity increases more strongly with ϕ for small crowders, slowing down the chain dynamics and reducing the looping rates. This non-trivial behaviour illustrated in Fig. 7 is our *first key result*.

Apart from the viscosity dependence, in Fig. 2 we highlight another important crowding-mediated effect. Namely, when the crowders are small, entropic effects favour a good mixing of crowders and chain monomers with little implications of the chain connectivity. When the crowders become larger, however, depletion effects become increasingly dominant. The chain becomes confined in a “cage”. We emphasise here that the cage is not static but rather a dynamic entity, because of perpetual diffusion of crowders. Only at very high ϕ values or with possible attractions between the crowders the cage becomes static, as studied in Ref.⁷⁴. In this confined state, the looping probability is significantly increased and thus the looping dynamics gets facilitated. As shown in Fig. 7 the depletion effect just outweighs the increased viscosity for larger crowders. The dynamics of crowders remains Brownian even at high volume fractions of $\phi \sim 0.3$, see below.

The unlooping time T_{ul} , in contrast, typically increases with ϕ . As shown in Figs. 7 and A.3c, while the dependence of T_{ul} on ϕ is very weak for large crowders, it becomes quite sizable for smaller crowders. The effect on T_{ul} is due to both the higher viscosity induced by MMC and the impeded chain opening imposed by the caging effects. For the unlooping process both effects do not lead to an inversion of the ϕ -dependence of T_{ul} inhibiting chain opening. The unlooping time is a monotonically decreasing function of the crowder size, see Fig. A.3d.¹¹⁷

D. Comparison with DNA hairpin formation experiments

Ref.⁶⁰ reports experimental data from fluorescence correlation measurements of ssDNA hairpin formation. The

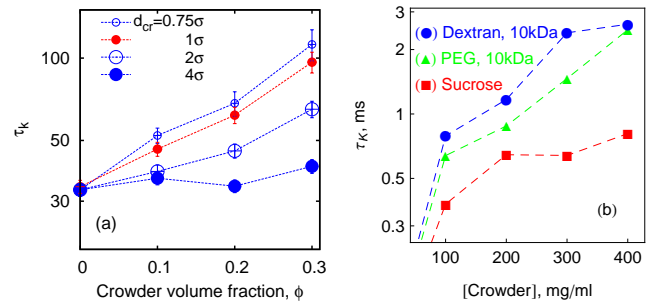


FIG. 8: Characteristic time τ_K given by Eq. (10) and computed from simulations (a) for $n = 16$ and $\epsilon_s = 5k_B T$. (b) Experimental data⁶⁰ for ssDNA hairpin formation kinetics in solutions of different crowders. Both graphs are in the log-linear scale.

characteristic time τ_K for the measured fluorescent blinking is given by the harmonic mean⁶⁰,

$$\tau_K = T_l T_{ul} / (T_l + T_{ul}). \quad (10)$$

Similar to the experimental data⁶⁰, we show that $\tau_K(\phi)$ has a tendency to grow with ϕ for crowders of all sizes and polymers of all lengths examined in the simulations, see Figs. 8 and A.7. We observe that the typical variation of τ_K with ϕ corresponds to a factor of 2-3, in agreement with the measured data⁶⁰, as shown in Fig. 8. We also reveal a systematic dependence of the crowder diameter onto τ_K enhancement, in which smaller crowders are most efficient, see Fig. 8. The curves in the plots indicate a nearly exponential dependence

$$\tau_K(\phi) \simeq \exp(\gamma\phi) \quad (11)$$

as function of the crowding fraction ϕ . This is consistent with the exponential dependence of the self-diffusivity of a tracer in crowded solutions, $D(\phi) \sim \exp(-\gamma\phi)$ ⁹⁵. We checked that looping of *longer* polymers in crowded solutions yield qualitatively similar enhancement effects on τ_K with ϕ , see Fig. A.7. In this figure the crowders are fairly large, $d_{cr} = 4 \times \sigma$, and the magnitude of τ_K enhancement is somewhat smaller, consistent with the behaviour of $\tau_K(d_{cr})$ presented in Fig. 8a.

To make the quantitative comparison of our results for τ_K to the experimentally observed $\tau_K(\phi)$ enhancement⁶⁰, one needs to compare the relative sizes of polymers and crowders (experiment versus simulations). Namely, 10 kDa PEG polymers have $R_{g,PEG} \approx 2.8$ nm, while for 21-bp long DNA hairpins $R_g \sim 7$ nm⁶⁰. In simulations, for $n = 16$ chains, see Fig. A.3, the gyration radius is $R_g \approx 2.5\sigma$ (Fig. 5b), so the crowders of diameter $d_{cr} \approx 2\sigma$ are in the same relation to the polymer size in simulations as 21-bp DNA hairpins to 10 kDa PEG in experiments⁶⁰. Note that 10 kDa branched dextran polymers are considerably smaller than 10 kDa PEG⁶⁰ and the dynamics of DNA hairpin formation is slower in dextran solutions. The physical reason for this behaviour, as

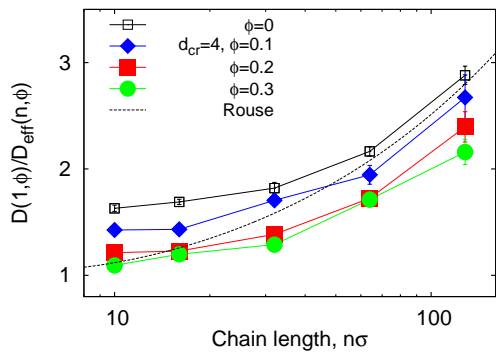


FIG. 9: Reciprocal effective diffusivity $D(1, \phi)/D_{\text{eff}}(n, \phi)$ of polymer ends, obtained from fit of the T_l data in Fig. 7 with Eq. 12. The Rouse chain result $D_R(n, 0)$ given by Eq. (13) with $D(1, 0) = 1/2$ as used in simulations is the dashed curve.

proposed in Ref.⁶⁰, is a pronounced sub-diffusion of DNA hairpins in solutions of dextran, with the scaling exponent of $0.7 < \beta < 0.85$, in stark contrast to the sucrose and PEG solutions where the hairpin diffusion is nearly Brownian ($0.9 < \beta < 1$), see also below.

E. Length dependence and effective diffusivity

The observed "tug-of-war" between facilitation and inhibition is a fundamental feature of the looping kinetics for all chain lengths. Fig. 7 illustrates that looping is systematically facilitated for larger crowdors and impeded for smaller crowdors. Concurrently, the scaling of the looping time with n given by Eq. (1) *does not* change appreciably in crowded solutions compared to the dilute case $\phi = 0$, as shown in Fig. 7. This is our *second important result*.

Note that for longer polymers the accessible space inside the coil increases and at some point even large crowdors can be accommodated therein, thus reverting effect of polymer compaction by MMC. However, the gyration radius of our longest chains with $n \approx 200$ monomers is still too small to see this happen for the larger crowdors ($d_{\text{cr}} = 4 \times \sigma$) studied. Thus, the $T_l(n)$ scaling behaviour for even longer chains remains similar to the situation in absence of crowdors.

We observe a slightly more pronounced looping time variation with ϕ for longer polymers in crowded solutions, in agreement with well-established results, for instance, in protein-DNA interactions². The unlooping times vary substantially with the polymer length (in stark contrast to the observations of Ref.¹¹). This indicates that the unlooping is not a purely local unbinding process, but it needs the cooperative motion of the polymer.¹¹⁸

In Fig. 9 we study how many chain monomers are involved in looping events by quantifying the inverse *effective* position-independent diffusivity $1/D_{\text{eff}}$ of the end

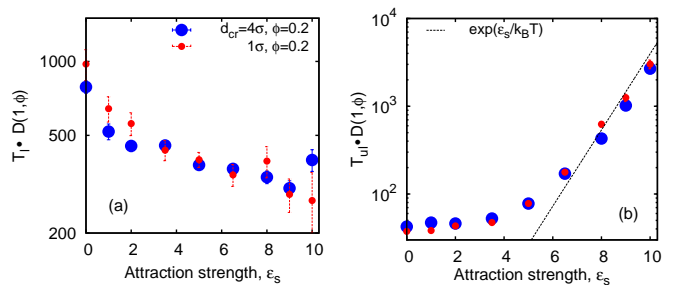


FIG. 10: Viscosity-renormalised looping (a) and unlooping times (b), namely $T_{l,ul} \rightarrow T_{l,ul}/\eta \sim T_{l,ul}D(1, \phi)$, at $\phi = 0.2$ for varying ϵ_s and $n = 32$. Note that with increase of ϵ_s the number of looping events for the same trace-length of $r(t)$ decreases, worsening the statistics.

monomers. We use the data of Fig. 7 for T_l and the general expression for mean first-passage (i.e., looping) times

$$T_l = \int_{r_c}^{r_{\text{eq}}} dr' \frac{e^{F(r')/(k_B T)}}{D_{\text{eff}}} \int_{r'}^{n\sigma} dr'' e^{-F(r'')/(k_B T)}, \quad (12)$$

in a general potential $F(r)$ ⁹⁶. Here $n\sigma$ is the maximal chain extension. We fit the simulation data for T_l with the free energy profiles $F(r)$ computed for each chain length in Fig. A.1. The effective end-to-end diffusivity in the model of Rouse chains without crowding as derived in Ref.¹⁶,

$$D_R(n, 0)/D(1, 0) \approx 8/\sqrt{\pi n} - 16/(3n), \quad (13)$$

is represented by the dashed line in Fig. 9. Although our simulation data in the limit $n \gg 1$ follow this Rouse-chain prediction, the diffusivity of the terminal fragments in the presence of crowdors for small n shows sizeable deviations.

The effective number of monomers involved in the looping dynamics $n_{\text{eff}} \propto D(1, \phi)/D_{\text{eff}}(n, \phi)$ increases slightly with n both for large and small crowdors, as shown in Fig. 9. This figure illustrates that the number of chain monomers participating in looping slightly but systematically decreases with the MMC fraction ϕ . The functional dependence of D_{eff} is qualitatively similar to that of Rouse chains at larger n , but with somewhat smaller D_{eff} values. For smaller n , however, a plateau of D_{eff} is observed for all chain lengths in simulations. For severe crowding we find that *less* monomers are involved in looping, compare the curves in Fig. 9. This analysis rationalises the *cooperativity* between the polymer extremities and the vicinal crowding particles. The ϕ -dependent chain end diffusivity is our *third main result*.¹¹⁹

F. Effects of the binding affinity

For ssDNA hairpins, the enthalpy gain of base-pairing upon looping is partly counter-balanced by the entropic

penalty^{104,105}. For instance, for the 21-bp hairpin with CCCAA/GGGTT termini in Ref.⁶⁰ the free energy of hairpin formation is $\sim 5k_B T^{73}$. This value is used in our simulations for the end-to-end binding energy ϵ_s , except for Fig. 10 where we vary ϵ_s in the broad range $0 \leq \epsilon_s \leq 10k_B T$. Larger ϵ_s values represent ssDNA hairpins with longer and thus more adhesive complementary end sequences. We observe a moderate, monotonic decrease of the looping time with ϵ_s . Moreover, for all ϵ_s values longer looping times are obtained for smaller crowders and faster looping is detected for larger crowders (Figs. 10 and A.8). This implies that our claims regarding the effects of crowding on the polymer looping dynamics are robust to changes of the model parameters.

Both looping and unlooping times can be rescaled by the effective solution viscosity $\eta \sim 1/D(1, \phi)$ to yield *universal* dependencies for different crowder sizes as demonstrated in Fig. 10b. Fig. A.8 shows the unscaled looping and unlooping data, together with the results for in absence of crowding, revealing the same trends for $T_{l,ul}$ with the crowder size as those presented for a fixed end-monomer affinity in Fig. 7b. The viscosity-based rescaling works particularly well for the unlooping. As expected, for large end-to-end attraction ϵ_s the unlooping time grows and exhibits Arrhenius-like kinetics,

$$T_l(\epsilon_s) \sim \exp[\epsilon_s/(k_B T)], \quad (14)$$

see the dotted line in Fig. 10b. These findings regarding the binding strength are our *fourth key result*. The exponential growth of the unlooping time with ϵ_s indicates the *local* physical nature of the unlooping process, in contrast to the looping kinetics at varying attractive strength ϵ_s which requires rather *large-scale* polymer re-organisations.

G. Cavity and Caging

To quantify the already mentioned caging effects imposed by the crowders on the polymer coil, we explicitly compute the distribution of crowders around the polymer, as illustrated in Fig. A.9. It shows that crowding particles of size comparable to the chain monomers diffuse quite substantially inside the coil volume. In contrast, crowders, whose size is much larger than the polymer monomers, are essentially excluded/depleted from the volume occupied by the polymer, thus facilitating polymer compaction and looping. Here, the reader is also referred to the investigation of caging effects in colloidal glasses⁷⁴.

We also evaluated the correlation characteristics of the number of contacts $m_{cr-p}(t)$ that the polymer chain establishes with the neighbouring crowders in the course of time, see Fig. A.10 for relatively large crowders. We define the normalised auto-correlation function of polymer-

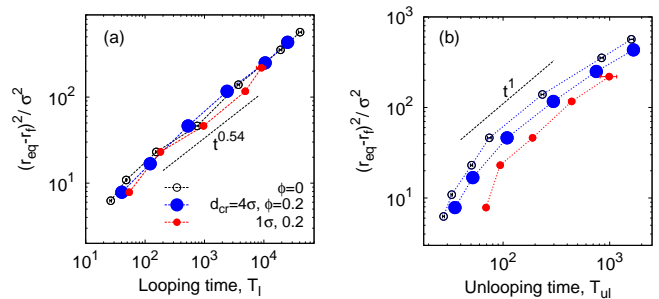


FIG. 11: Diffusion law of Eq. (18) for looping and unlooping times of the chain ends necessary to bridge the distance $\langle \delta r(n)^2 \rangle$. The asymptote of Eq. (19) is the dotted line in panel (a); a linear scaling in panel (b) as a guide for the eye. Parameters are the same as in Fig. 7 and $\phi = 0.2$.

crowders contacts as²⁵

$$\text{ACF}(\Delta) = \frac{\langle m_{cr-p}(t + \Delta) m_{cr-p}(t) \rangle - \langle m_{cr-p}(t + \Delta) \rangle \langle m_{cr-p}(t) \rangle}{\langle m_{cr-p}(t)^2 \rangle - \langle m_{cr-p}(t) \rangle^2}, \quad (15)$$

where the angular brackets denote averaging along the $m_{cr-p}(t)$ trace. The critical distance between the centres of polymer monomers and neighbouring crowders in the algorithm is set to $R_c = \sigma/2 + d_{cr}$, such that at most one crowder fits between a crowder and a polymer monomer in contact. We checked that the observed ACF(Δ) decay length is only weakly sensitive to the chosen critical contact distance R_c .

We observe that, after an initial fast decrease of the number of contacts established, the further decay of the correlation function becomes nearly exponential, $\text{ACF}(\Delta) \sim \exp[-\Delta/T^*]$, see Fig. A.10. The corresponding decay length T^* increases for longer polymers, partly due to a larger number of overall contacts m_{cr-p} established. The characteristic time scale T^* we obtain here is substantially *shorter* than the polymer looping time T_l at the same conditions, compare Fig. 7 and Fig. A.10.¹²⁰

IV. RESULTS: DIFFUSION

A. Subdiffusion of polymer ends

MMC may impede the folding dynamics of short polypeptides due to a higher solution viscosity⁹⁷ overwhelming the looping-facilitating caging effects. A size-dependent diffusivity emerges⁹⁷: the diffusion of longer chains is impeded more strongly. Fig. 11 based on our simulations shows a similar effect for the mean squared looping distance versus the looping and unlooping times. This quantifies the diffusion law for looping events, i.e., the diffusive bridging of the distance

$$\delta r = r_{eq} - r_c \quad (16)$$

from the equilibrium distance r_{eq} of the sticky ends to the looped state with end-to-end distance r_c , and vice versa. As function of the chain length n , we checked that, similar to R_g in Fig. 6b, for longer polymers the scaling law

$$\langle \delta r(n) \rangle^2 \sim n^{2\nu} \quad (17)$$

is fulfilled. From the mean times T_l and T_{ul} we compute the scaling exponents α from the generalised diffusion law⁹⁸

$$\langle \delta r(n)^2 \rangle = 2D_{\alpha_l} \langle T_l(n) \rangle^{\alpha_l} = 2D_{\alpha_{ul}} \langle T_{ul}(n) \rangle^{\alpha_{ul}}. \quad (18)$$

Here D_{α_i} is the generalised diffusion coefficient in units of $\text{cm}^2 \text{sec}^{-\alpha_i}$ and α_i the anomalous diffusion exponent for looping and unlooping processes, respectively. This approach helps us to distinguish the effects of the enhanced viscosity at higher ϕ from excluded-volume effects of crowders. Fig. 11a illustrates that at large ϕ the looping dynamics is subdiffusive with $0.5 \lesssim \alpha_l \lesssim 0.6$. This is but the standard result for polymer looping, as seen from combination of Eqs. (1) and (18),

$$\langle \delta r(n)^2 \rangle \sim T_l(n)^{2\nu/(2\nu+1)} \sim T_l(n)^{0.54}. \quad (19)$$

In contrast, for polymer unlooping no power-law scaling is found in the range of chain lengths $n\sigma$ considered here, see Fig. 11b. This fact is related to the absence of a power-law scaling in the $T_{ul}(n)$ dependence, see Fig. 7b.

These observations can be rationalised as follows. Once a thermal fluctuation breaks the bond between the sticky ends, the separation r of the polymer ends drifts downhill in the free energy landscape $F(r)$ discussed above, quickly assuming larger values. In contrast, the looping time depends strongly on n : to loop, the polymer needs to overcome an entropic penalty to get from r_{eq} to the contact distance r_c , see Fig. A.1. Thus, for looping it takes much longer to bridge the distance $\delta r(n)$ and involves interactions with a larger number of surrounding crowders, effecting the power law (19) with the small value $\alpha_l = 0.54$.

B. Diffusion of a tracer particle

The size of the obstacles controls the facilitation or inhibition of polymer looping in crowded environments. Additionally, we exploit how fast the polymer ends join one another from the extended equilibrium state and reveal the regime of anomalous diffusion for the looping times with the scaling exponent of ≈ 0.54 , see Eq. (19). Here we briefly examine whether this sub-diffusive behaviour of extended polymer extremities is connected to any subdiffusion of an *isolated tracer particle* in the crowded solutions simulated.

We compute the mean square displacement (MSD) for the diffusion of a single monomer of the chain (tracer particle), $\langle s^2(t) \rangle$, in crowded solutions with varying MMC

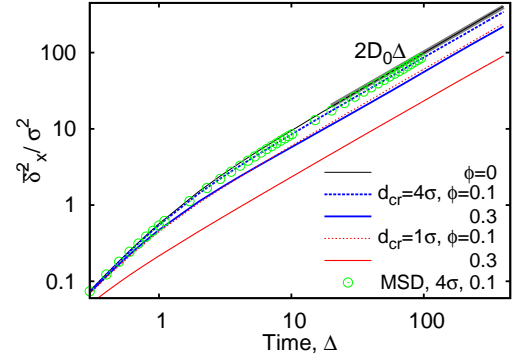


FIG. 12: MSD $\langle s^2(t) \rangle$ (green symbols) and time averaged MSD $\langle \overline{\delta_x^2(\Delta)} \rangle$ along one spatial directions computed for varying crowder size and MMC fractions ϕ (as indicated in the plot). For each set of parameters, we average over $N = 5$ time series for $\langle \overline{\delta^2} \rangle$ and over $N = 10^3$ traces for the MSD. The asymptote $\text{MSD}_x(t) = 2Dt$ is the thick solid line, where $D = D(1, 0)$ is the single monomer free space diffusivity.

fraction ϕ and crowder diameter d_{cr} . Namely, we use the anomalous diffusion law⁹⁸⁻¹⁰¹

$$\langle s^2(t) \rangle \sim t^\beta \quad (20)$$

to compute the local scaling exponent

$$\beta(t) = d[\log(\langle s^2(t) \rangle)] / d[\log(t)] \quad (21)$$

along the ensemble averaged MSD trajectory. For the Brownian motion $\beta(t) \equiv 1$ at all times.

We find that the viscosity of solutions of smaller crowders grows with ϕ faster than for larger obstacles, see Fig. A.6. In this figure, the diffusivity has been extracted from the time averaged MSD along x -direction,

$$\overline{\delta_{x,i}^2(\Delta)} = \frac{1}{t - \Delta} \int_0^{t-\Delta} [x_i(t' + \Delta) - x_i(t')]^2 dt', \quad (22)$$

in the lag time interval of $40 < \Delta < 400$, i.e., in the region where the linear scaling of the time average MSD is clearly established. This fast increase of the tracer's viscosity is consistent with the experimental measurements in crowded dextran solutions, see Fig. 5b in Ref.¹⁰². In the latter, the tracer exhibits an exponential growth of micro-viscosity with concentration of polymeric crowders, valid for a wide range of relative tracer-crowder dimensions. The growth of viscosity with MMC fraction ϕ is also in accord with theoretical predictions¹⁰³.

The MSD and ensemble averaged time averaged MSD $\langle \overline{\delta_x^2(\Delta)} \rangle = N^{-1} \sum_{i=1}^N \overline{\delta_{x,i}^2(\Delta)}$ traces are identical in the long-time limit, see Fig. 12, with the long-time exponent β being close to unity (Brownian motion). This indicates the *ergodic* tracer diffusion in the crowded solutions implemented in our simulations yields subdiffusive motion

of the chain ends. In Fig. 12 we also show the ensemble and time averaged MSDs of a tracer particle with unit diameter in the crowded solutions. The diffusion exponent is nearly unity and no disparity of ensemble and time averaged displacements is detected, i.e., the motion is ergodic^{99,101}.

V. DISCUSSION

MMC non-specifically favours more compact conformations of proteins and speeds up their folding kinetics²¹, as well as stabilises the proteins against thermal denaturation⁹⁵. MMC may also reduce the occurrence of mis-folded states via reduction of the conformational space³⁸. The degree of crowding in living cells is heterogeneous and the crowdors are polydisperse in size¹⁰⁷, giving rise to a micro-compartmentalisation of the cellular cytoplasm^{106,108,109}. These effects pose the questions whether other fundamental elements of gene expression in biological cells are equally affected by MMC.

Specifically, recent gene-regulation experiments² have shown that bigger dextran molecules increase the rates of gene expression by RNA Polymerase to a higher-fold as compared to smaller ones². Bigger dextran molecules both reduce the diffusivity of RNA Polymerase and enhance the number of binding events to the promoters (enhancing the association and reducing the dissociation rates). In solution of small crowdors the impact of ϕ on gene expression rates is non-monotonic (due to a compensation of moderate effects of MMC on Polymerase diffusivity and its association rate to the DNA sites). In contrast, in solution of bigger crowdors the expression rate grows monotonically and strongly with the ϕ fraction².

Here we show that indeed the looping kinetics of polymers such as DNA is highly sensitive to the volume fraction and size of crowdors in a non-trivial way, and a quantitative knowledge of this effect is necessary for the understanding of the molecular biological function of DNA based on looping. From extensive Langevin dynamics simulations we demonstrated that polymer looping is facilitated in the presence of large crowdors, mainly due to depletion-based chain compaction. In contrast, for small crowdors the dominant effect is the larger effective viscosity impeding the looping dynamics. The exact tradeoff between the two effects critically depends on the system parameters.

Our results are applicable to generic DNA looping and RNA folding dynamics in crowded systems¹¹⁰, particularly, the formation of ssDNA hairpins with in vitro crowdors⁶⁰. Here, our predictions for crowder size and binding affinity effects can be tested directly in experiments. We already have showed that some predictions of our model indeed capture the experimental behaviour⁶⁰. As targets for future studies, crowdors of particular surface properties, non-inert poly-disperse and aspherical

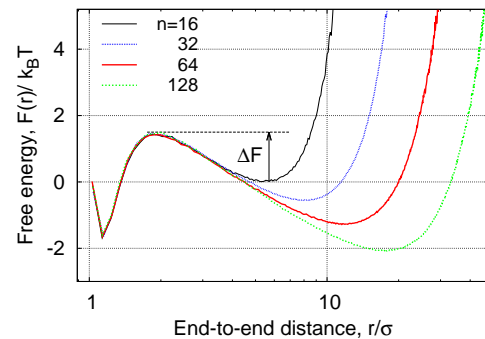


FIG. A.1: The free energy landscape $F(r)$ for polymer looping for varying chain length at $\phi = 0.2$ and $d_{cr} = 4\sigma$. The energy minima at small end-to-end distances are aligned in the plot in order to assess the barriers heights for looping, $\Delta F(n)$.

crowdors will be studied⁸⁹.

In addition, the simulations of semi-flexible instead of flexible polymers in the presence of both MMC and external spherical confinement are expected to reveal a number of novel features. For instance, in contrast to free-space flexible chains, the presence of spacial restrictions and finite bending energy penalty upon polymer looping yields a quasi-periodic but *highly erratic* dependence with the chain length $n\sigma$. Strong anti-correlation of the looping time and looping probability versus the polymerisation degree, pertinent for flexible chains, as those presented in Figs. 6a and 7a, become more profound for the dynamics of cavity-confined semi-flexible polymers, see Ref.⁸⁹. We hope that our current investigation triggers new theoretical and experimental developments of static and dynamical properties of polymers in the crowded realm omnipresent in the interior of living cells.¹²¹

Acknowledgments

We thank D. Jost for discussions. We acknowledge funding from the Academy of Finland (FiDiPro scheme to RM), the Deutsche Forschungsgemeinschaft (DFG Grant CH 707/5-1 to AGC), and the Federal Ministry of Education and Research (BMBF Project to JS). We are particularly grateful to an anonymous referee for the insightful comments which improved our understanding of the subject.

Appendix A

In this Appendix we present the supplementary figures explaining the details of our main-text results.

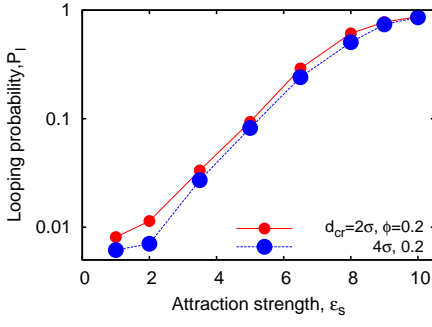


FIG. A.2: Looping probability versus terminal monomer stickiness, computed for $n = 32$ chains at different crowder size at $\phi = 0.2$.

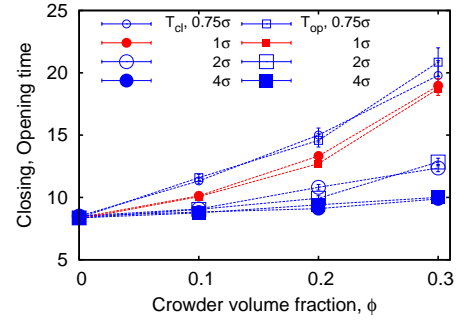


FIG. A.5: Opening and closing times $T_{op,cl}$ versus MMC fraction ϕ for varying crowder size. Parameters are the same as in Fig. A.3.

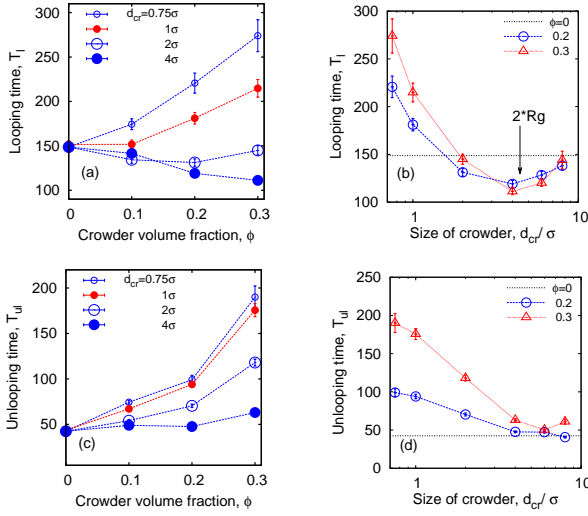


FIG. A.3: Looping and unlooping times versus ϕ , computed for a varying crowder size d_{cr} , for short chains with $n = 16$ monomers, and $\epsilon_s = 5k_B T$.

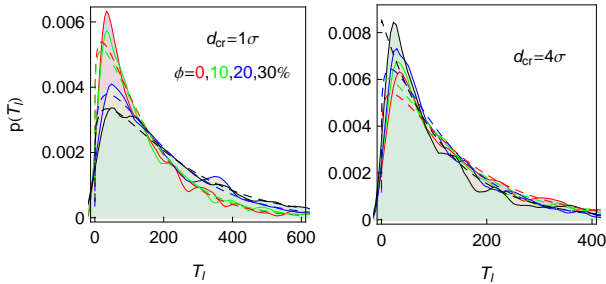


FIG. A.4: The PDFs of looping times for $n = 16$, $\epsilon_s = 5k_B T$ and crowder sizes and fractions as indicated. Smoothed histograms are the simulations data and the dashed curves of the respective colour are the fits by Eq. (9). The slight bumpiness of the histograms is due to the limited statistics of the generated looping events.

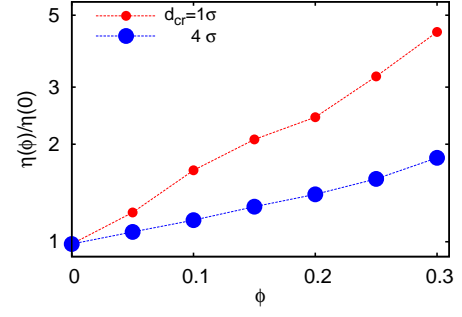


FIG. A.6: Effective solution viscosity $\eta(\phi) = k_B T / (3\pi\sigma D(1, \phi))$ for a tracer of diameter 1σ in solutions with varying crowder diameter d_{cr} , as extracted from the analysis of time averaged MSD traces.

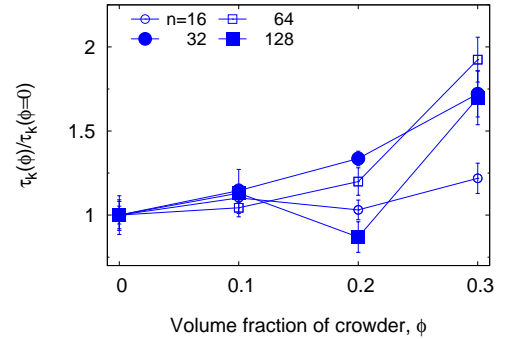


FIG. A.7: The normalised $\tau_K(\phi)$ for varying chain length n , plotted for $\epsilon_s = 5k_B T$ end-monomer adhesion strength and relatively big crowders $d_{cr} = 4\sigma$. For small crowders the effect ϕ on the enhancement of τ_K is stronger and more systematic (not shown).

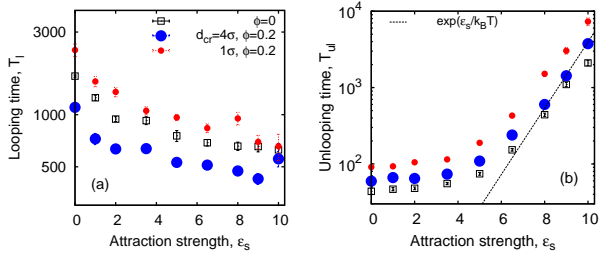


FIG. A.8: The same data as in Fig. 10 but without normalisation by the effective viscosity of the solution, $\eta(\phi) \sim 1/D(1, \phi)$. The data-set for the uncrowded solution is also included (open symbols).

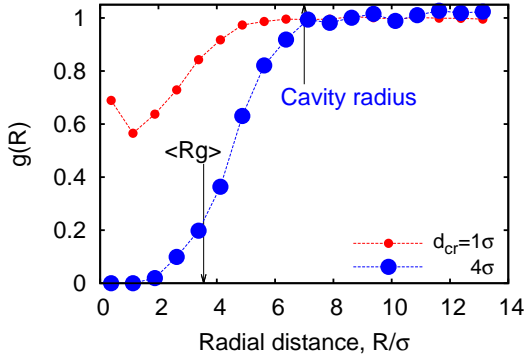


FIG. A.9: The radial distribution function of relatively small (red dots) and large (blue dots) crowders around a polymer coil with $n = 32$ monomers at MMC fraction of $\phi = 0.1$.

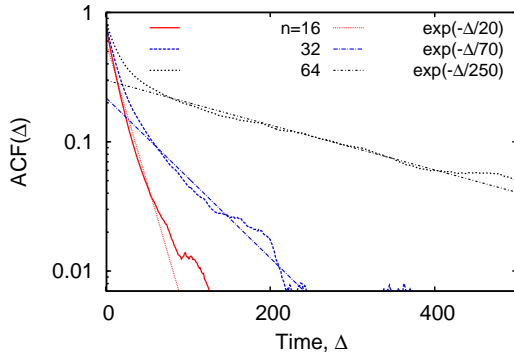


FIG. A.10: The auto-correlation function of the polymer-crowders contact number (15), computed for polymers of varying length, at $\phi = 0.2$ and $d_{cr} = 4\sigma$. The corresponding exponential asymptotes are shown as the dotted lines.

- * Electronic address: rmetzler@uni-potsdam.de
- ¹ Golding I, Cox EC (2006) Physical nature of bacterial cytoplasm. *Phys Rev Lett* 96:098102.
 - ² Tan C, Saurabh S, Bruchez MP, Schwartz R, LeDuc P (2013) Molecular crowding shapes gene expression in synthetic cellular nanosystems. *Nature Nanotech* 8:602–608.
 - ³ Philips R, Kondev J, Theriot J, Garcia H (2012) Physical biology of the cell. Garland Science, New York.
 - ⁴ Morelli MJ, ten Wolde PR, Allen RJ (2009) DNA looping provides stability and robustness to the bacteriophage λ switch. *Proc Natl Acad Sci USA* 106(20):8101–8106.
 - ⁵ Li, GW, Berg OG, Elf J (2009) Effects of macromolecular crowding and DNA looping on gene regulation kinetics. *Nature Phys* 5(4):294–297.
 - ⁶ Matsuda H, Putzel GG, Backman, V, Szleifer, I (2014) Macromolecular Crowding as a Regulator of Gene Transcription. *Biophys J* 106(4):1801–1810.
 - ⁷ Wilemski G, Fixman M (1974) Diffusion-controlled intrachain reactions of polymers. *J Chem Phys* 60(3):866–877.
 - ⁸ Guérin T, Bénichou O, Voituriez R (2013) Reactive conformations and non-Markovian cyclization kinetics of a Rouse polymer. *J Chem Phys* 138(9):094908.
 - ⁹ Guérin T, Bénichou O, Voituriez R (2012) Non-Markovian polymer reaction kinetics. *Nature Chem* 4(7):568–573.
 - ¹⁰ Szabo A, Schulten K, Schulten Z (1980) First passage time approach to diffusion controlled reactions. *J Chem Phys* 72(8):4350–4357.
 - ¹¹ Toan NM, Marenduzzo D, Cook PR, Micheletti C (2006) Depletion effects and loop formation in self-avoiding polymers. *Phys Rev Lett* 97(17):178302.
 - ¹² Shin J, Sung W (2012) Effects of static and temporally fluctuating tensions on semiflexible polymer looping. *J Chem Phys* 136(4):045101.
 - ¹³ Fritsche M, Heermann DW (2011) Confinement driven spatial organization of semiflexible ring polymers: Implications for biopolymer packaging. *Soft Matter* 7:6906–6913.
 - ¹⁴ Stampe J, Sokolov IM (2001) Cyclization of a polymer with charged reactive end groups. *J Chem Phys* 114(11):5043–5048.
 - ¹⁵ Cheng RR, Makarov DE (2011) Failure of one-dimensional Smoluchowski diffusion models. *J Chem Phys* 134(8):085104.
 - ¹⁶ Toan NM, Morrison G, Hyeon C, Thirumalai D (2008) Kinetics of loop formation in polymer chains. *J Phys Chem B* 112(19):6094–6106.
 - ¹⁷ Klenin KV, Langowski J (2004) Modeling of intramolecular reactions of polymers: An efficient method based on Brownian dynamics simulations. *J Chem Phys* 121(10):4951–4960.
 - ¹⁸ Kim JS, Backman V, Szleifer I (2011) Crowding-induced structural alterations of random-loop chromosome model. *Phys Rev Lett* 106(16):168102.
 - ¹⁹ Marenduzzo D, Finan K, Cook PR (2006) The depletion attraction: an under-appreciated force driving cellular organization. *J Cell Biol* 175(5):681–686.
 - ²⁰ Marenduzzo D, Micheletti C, Cook PR (2006) Entropy-driven genome organization. *Biophys J* 90(10):3712–3721.
 - ²¹ Zhou HX, Rivas G, Minton AP (2008) Macromolecular crowding and confinement: biochemical, biophysical, and potential physiological consequences. *Ann Rev Biophys* 37:375–397.
 - ²² Bräuchle C, Lamb DC, Michaelis J (2012) Single Particle Tracking and Single Molecule Energy Transfer (Wiley-VCH, Weinheim, Germany).
 - ²³ Micheletti C, Marenduzzo D, Orlandini E (2011) Polymers with spatial or topological constraints: theoretical and computational results. *Phys Rep* 504(1):1–73.
 - ²⁴ Dorier J, Stasiak A (2013) Modelling of crowded polymers elucidate effects of double-strand breaks in topological domains of bacterial chromosome *Nucl Acids Res* 41(14):6808–6815.
 - ²⁵ Shin J, Cherstvy AG, Metzler R (2014) Mixing and segregation of ring polymers: spatial confinement and molecular crowding effects, *New J Phys* 16:053047.
 - ²⁶ Cremer T, Cremer M (2010) Chromosome territories. *Cold Spring Harbor Persp Biol*, 2(3):a003889.
 - ²⁷ Le T B, Imakaev MV, Mirny LA, Laub MT (2013) High-resolution mapping of the spatial organization of a bacterial chromosome. *Science* 342(6159):731–734.
 - ²⁸ Denton AR (2014) Crowding in polymer-nanoparticle mixtures. *Int Rev Cell Mol Biol* 307:27–71.
 - ²⁹ Höfling F, Franosch T (2013) Anomalous transport in the crowded world of biological cells. *Rep Prog Phys* 76(4):046602.
 - ³⁰ Weiss M (2014) Crowding, Diffusion, and Biochemical Reactions. *Int Rev Cell Mol Biol* 307:383–417.
 - ³¹ Zimmerman SB, Minton AP (1993) Macromolecular crowding: biochemical, biophysical, and physiological consequences. *Ann Rev Biophys Biomol Struct* 22(1):27–65.
 - ³² McGuffee SR, Elcock AH (2010) Diffusion, crowding & protein stability in a dynamic molecular model of the bacterial cytoplasm. *PLoS Comput Biol* 6(3):e1000694.
 - ³³ Szymanski J and Weiss M (2009) Elucidating the origin of anomalous diffusion in crowded fluids. *Phys Rev Lett* 103:038102.
 - ³⁴ Pan W, Filobelo L, Pham NDP, Galkin O, Uzunova VV, Vekilov PG (2009) Viscoelasticity in homogeneous protein solutions. *Phys Rev Lett* 102:058101.
 - ³⁵ Hu CK, Li MS (2013) Dual effect of crowders on fibrillation kinetics of polypeptide chains revealed by lattice models. *J Chem Phys* 138(18):185101.
 - ³⁶ Schreiber G, Haran G, Zhou HX (2009) Fundamental aspects of protein-protein association kinetics. *Chem Rev* 109(3):839–860.
 - ³⁷ Erlkamp M, Grobelny S, Winter R (2014) Crowding effects on the temperature and pressure dependent structure, stability and folding kinetics of Staphylococcal Nuclease. *Phys Chem Chem Phys* 16(13):5965–5976.
 - ³⁸ Cheung MS, Klimov D, Thirumalai D (2005) Molecular crowding enhances native state stability and refolding rates of globular proteins. *Proc Natl Acad Sci USA* 102(13):4753–4758.
 - ³⁹ Hyeon C, Thirumalai D (2011) Capturing the essence of folding and functions of biomolecules using coarse-grained models. *Nature Comm* 2(487):1–11.
 - ⁴⁰ Guo M, Xu Y, Gruebele M (2012) Temperature dependence of protein folding kinetics in living cells. *Proc Natl Acad Sci USA* 109(44):17863–17867.
 - ⁴¹ del Alamo M, Rivas G, Mateu MG (2005) Effect of macromolecular crowding agents on human immunodeficiency

- virus type 1 capsid protein assembly in vitro. *J Virol* 79(22):14271–14281.
- ⁴² Denesyuk NA, Thirumalai D (2011) Crowding promotes the switch from hairpin to pseudoknot conformation in human telomerase RNA. *J Am Chem Soc* 133(31):11858–11861.
- ⁴³ Weigel AV, Simon B, Tamkun MM, Krapf D (2011) Ergodic and nonergodic processes coexist in the plasma membrane as observed by single-molecule tracking. *Proc Natl Acad Sci USA* 108(16):6438–6443.
- ⁴⁴ Jeon JH, Monne HMS, Javanainen M, Metzler R (2012) Anomalous diffusion of phospholipids and cholesterol in lipid bilayer and its origins. *Phys Rev Lett* 109:188103.
- ⁴⁵ Javanainen M, Hammaren H, Monticelli L, Jeon JH, Metzler R, Vattulainen I (2013) Anomalous and normal diffusion of proteins and lipids in crowded lipid membranes. *Faraday Disc* 161:397–417.
- ⁴⁶ Mahynski NA, Irick B, Panagiotopoulos AZ (2013) Structure of phase-separated athermal colloid-polymer systems in the protein limit. *Phys. Rev. E* 87:022309.
- ⁴⁷ Paricaud P, Varga S, Jackson G (2003) Study of the demixing transition in model athermal mixtures of colloids and flexible self-excluding polymers using the thermodynamic perturbation theory of Wertheim. *J. Chem. Phys.* 118(8):8525–8536.
- ⁴⁸ Swigon D, Coleman BD, Olson WK (2006) Modeling the Lac repressor-operator assembly: the influence of DNA looping on Lac repressor conformation. *Proc Natl Acad Sci USA* 103(26):9879–9884.
- ⁴⁹ Priest DG, Cu L, Kumar S, Dunlap DD, Dodd IB, Shearwin KE (2014) Quantitation of the DNA tethering effect in long-range DNA looping in vivo and in vitro using the Lac and λ repressors. *Proc Natl Acad Sci USA* 111(1):349–354.
- ⁵⁰ Hensel Z, Weng X, Lagda AC, Xiao J (2013) Transcription-factor-mediated DNA looping probed by high-resolution, single-molecule imaging in live *E. coli* cells. *PLoS Biol* 11(6):e1001591.
- ⁵¹ van den Broek B, Lomholt MA, Kalisch SM, Metzler R, Wuite GJ (2008) How DNA coiling enhances target localization by proteins. *Proc Natl Acad Sci USA* 105(41):15738–15742.
- ⁵² Lomholt MA, van den Broek B, Kalisch SMJ, Wuite GJL, Metzler R (2009) Facilitated diffusion with DNA coiling. *Proc Natl Acad Sci USA* 106(20):8204–8208.
- ⁵³ ten Wolde PR, Mugler A (2013) Importance of crowding in signaling, genetic, and metabolic networks. *Intl Rev Cell Mol Biol*, 307:419–442.
- ⁵⁴ Tabaka M, Kalwarczyk T, Holyst R (2014) Quantitative influence of macromolecular crowding on gene regulation kinetics. *Nucl Acids Res* 42(2):727–738.
- ⁵⁵ Cherstvy AG, Teif VB (2013) "Structure-driven homology pairing of chromatin fibers: the role of electrostatics and protein-induced bridging", *J Biol Phys* 39(3):363–385.
- ⁵⁶ Zhou H X (2008) Protein folding in confined and crowded environments. *Arch Biochem Biophys* 469(1):76–82.
- ⁵⁷ Dupuis NF, Holmstrom ED, Nesbitt DJ (2014) Molecular-crowding effects on single-molecule RNA folding/unfolding thermodynamics and kinetics. *Proc Natl Acad Sci USA* 111(23):8464–8469.
- ⁵⁸ Bonnet G, Krichinsky O, Libchaber A (1998) Kinetics of conformational fluctuations in DNA hairpin-loops. *Proc Natl Acad Sci USA* 95(15):8602–8606.
- ⁵⁹ Frederickx R, in't Veld T, Carlon E (2014) Anomalous Dynamics of DNA Hairpin Folding. *Phys Rev Lett* 112:198102.
- ⁶⁰ Stiehl O, Weidner-Hertrampf K, Weiss M (2013) Kinetics of conformational fluctuations in DNA hairpin-loops in crowded fluids. *New J Phys* 15(11):113010.
- ⁶¹ B. Lu and A. R. Denton (2011) Crowding of polymer coils and demixing in nanoparticle-polymer mixtures *J Phys: Condens Matter* 23(28):285102.
- ⁶² Kudlay A, Hyeon C, Thirumalai D (2012) Influence of the Shape of Crowding Particles on the Structural Transitions in a Polymer. *J Phys Chem B* 116(29):8513–8522.
- ⁶³ Denton AR, Schmidt M (2005) Mixtures of charged colloid and neutral polymer: Influence of electrostatic interactions on demixing and interfacial tension. *J Chem Phys* 122(24):244911.
- ⁶⁴ Denton AR (2014) Crowding in polymer-nanoparticle mixtures. *Int Rev Cell Mol Biol* 307:27–71.
- ⁶⁵ Lee NK, Abrams CF, Johner A (2005) Optimal confinement for internal polymer binding. *EPL* 72(6):922–928.
- ⁶⁶ Abrams CF, Lee NK, Johner A (2006) Diffusion-reaction in confined polymer chains. *Macromolecules* 39(10):3655–3663.
- ⁶⁷ Kremer K, Grest GS (1990) Dynamics of entangled linear polymer melts: A molecular dynamics simulation, *J Chem Phys* 92:5057–5086.
- ⁶⁸ Bhattacharyya P, Sharma R, Cherayil BJ (2012) Confinement and viscoelastic effects on chain closure dynamics. *J Chem Phys* 136(23):234903.
- ⁶⁹ Shin J, Cherstvy AG, Metzler R (2014) Sensing viruses by mechanical tension of DNA in responsive hydrogels, *Phys Rev X* 4:021002.
- ⁷⁰ Shore D, Langowski J, Baldwin RL (1981) DNA flexibility studied by covalent closure of short fragments into circles. *Proc Natl Acad Sci USA* 78(8):4833–4837.
- ⁷¹ Vologodskii A, Frank-Kamenetskii MD (2013) Strong bending of the DNA double helix. *Nucl Acids Res* 41(14):6785–6792.
- ⁷² Mahynski NA, Panagiotopoulos AZ, Meng D, Kumar SK (2014) Stabilizing colloidal crystals by leveraging void distributions. *Nature Comm* 5:4472.
- ⁷³ Jost D, Everaers R (2009) A Unified Poland-Scheraga Model of Oligo- and Polynucleotide DNA Melting: Salt Effects and Predictive Power. *Biophys J* 96(3):1056–1067.
- ⁷⁴ Zaccarelli E, Poon WCK (2009) Colloidal glasses and gels: The interplay of bonding and caging, *Proc Natl Acad Sci USA* 106(36):15203–15208.
- ⁷⁵ SantaLucia Jr. J (1998) A unified view of polymer, dumbbell, and oligonucleotide DNA nearest-neighbor thermodynamics. *Proc Natl Acad Sci USA* 95(4):1460–1465.
- ⁷⁶ Chen Y, Luo K (2013) Dynamics of polymer translocation through a nanopore induced by different sizes of crowding agents. *J Chem Phys* 138(20):204903.
- ⁷⁷ Cherstvy AG (2011) DNA cyclization: suppression or enhancement by electrostatic repulsions? *J Phys Chem B* 115(15):4286–4294.
- ⁷⁸ Nakano SI, Miyoshi D, Sugimoto N (2013) Effects of Molecular Crowding on the Structures, Interactions, and Functions of Nucleic Acids. *Chem Rev* 114(5):2733–2758.
- ⁷⁹ Ando T, Chow E, Skolnick J (2013) Dynamic simulation of concentrated macromolecular solutions with screened long-range hydrodynamic interactions: Algorithm and limitations. *J Chem Phys* 139(12):121922.
- ⁸⁰ Winkler RG (1999) Analytical calculation of the relaxation dynamics of partially stretched flexible chain

- molecules: necessity of a worm-like chain description. *Phys Rev Lett* 82(9):1843–1846.
- ⁸¹ Winkler RG, Keller S, Rädler JO (2006) Intramolecular dynamics of linear macromolecules by fluorescence correlation spectroscopy. *Phys Rev E* 73(4):041919.
- ⁸² Shusterman R, Alon S, Gavrinov T, Krichevsky O (2004) Monomer Dynamics in Double- and Single-Stranded DNA Polymers. *Phys Rev Lett* 92(4):048303.
- ⁸³ Petrov EP, Ohrt T, Winkler RG, Schwille R (2006) Diffusion and segmental dynamics of double-stranded DNA. *Phys Rev Lett* 97(25):258101.
- ⁸⁴ Smith DE, Chu S (1998) Response of Flexible Polymers to a Sudden Elongational Flow. *Science* 281(5381):1335–1340.
- ⁸⁵ Perkins TT, Quake SR, DE Smith, S Chu (1994) Relaxation of a single DNA molecule observed by optical microscopy. *Science* 264(5160):822–826.
- ⁸⁶ Chemla YR, Ha T (2014) Ultraslow relaxation of confined DNA. *Science* 345(6195):380–381.
- ⁸⁷ von Hansen Y, Hinczewski M, Netz RR (2011) Hydrodynamic screening near planar boundaries: Effects on semiflexible polymer dynamics. *J Chem Phys* 134:235102.
- ⁸⁸ Schreiber G, Haran G, Zhou HX (2009) Fundamental aspects of protein-protein association kinetics. *Chem Rev* 109(3):839–860.
- ⁸⁹ Shin J, Cherstvy AG, Metzler R, work in progress.
- ⁹⁰ Grosberg AY, Khokhlov AR (1994) Statistical physics of macromolecules (AIP Press, Woodbury, NY).
- ⁹¹ Li X, Kolomeisky AB (2013) Mechanisms and topology determination of complex chemical and biological network systems from first-passage theoretical approach. *J Chem Phys* 139(14):144106.
- ⁹² Valleriani A, Li X, Kolomeisky AB (2014) Unveiling the hidden structure of complex stochastic biochemical networks, *J Chem Phys* 140(6):064101.
- ⁹³ Chung HS, Louis, JM, Eaton WA (2009) Experimental determination of upper bound for transition path times in protein folding from single-molecule photon-by-photon trajectories. *Proc Natl Acad Sci USA* 106(29):11837–11844.
- ⁹⁴ Neupane K, Ritchie DB, Yu H, Foster DA, Wang F, Woodside MT (2012) Transition path times for nucleic acid folding determined from energy-landscape analysis of single-molecule trajectories. *Phys Rev Lett* 109(6):068102.
- ⁹⁵ Minton KW, Karmin P, Hahn GM, Minton AP (1982) Nonspecific stabilization of stress-susceptible proteins by stress-resistant proteins. *Proc Natl Acad Sci USA* 79(23):7107–7111.
- ⁹⁶ Van Kampen NG (2007) *Stochastic Processes in Physics and Chemistry*, Third Edition, North Holland.
- ⁹⁷ Mukherjee S, Waegle MM, Chowdhury P, Guo L, Gai F (2009) Effect of macromolecular crowding on protein folding dynamics at the secondary structure level. *J Mol Biol* 393(1):227–236.
- ⁹⁸ Metzler R, Klafter J (2000) The random walk’s guide to anomalous diffusion: a fractional dynamics approach. *Phys Rep* 339(1):1–77.
- ⁹⁹ Barkai E, Garini Y, Metzler R (2012) Strange kinetics of single molecules in living cells. *Phys Today* 65(8):29–35.
- ¹⁰⁰ Metzler R, Klafter J (2004) The restaurant at the end of the random walk: recent developments in the description of anomalous transport by fractional dynamics. *J Phys A: Math Gen* 37(31):R161–R208.
- ¹⁰¹ Metzler R, Jeon JH, Cherstvy AG, Barkai E (2014) Anomalous diffusion models and their properties: non-stationarity, non-ergodicity, and ageing at the centenary of single particle tracking, *Phys Chem Chem Phys* 16:???–??? (2014). DOI: 10.1039/C4CP03465A
- ¹⁰² Goins AB, Sanabria H, Waxham MN (2008) Macromolecular Crowding and Size Effects on Probe Microviscosity. *Biophys J* 95(11):5362–5373.
- ¹⁰³ Minton AP (2012) Hard Quasi-spherical Particle Models for the Viscosity of Solutions of Protein Mixtures. *J. Phys. Chem. B* 116(31):9310–9315.
- ¹⁰⁴ Kuznetsov SV, Shen Y, Benight AS, Ansari A (2001) A Semiflexible Polymer Model Applied to Loop Formation in DNA Hairpins, *Biophys J* 81(5):2864–2875.
- ¹⁰⁵ Woodside MT et al (2005) Nanomechanical measurements of the sequence-dependent folding landscapes of single nucleic acid hairpins. *Proc Natl Acad Sci USA* 103(16):6190–6195.
- ¹⁰⁶ ”Microcompartmentation and Phase Separation in Cytoplasm”, A Survey of Cell Biology, Eds.: H. Walter, D. Brooks, and P. Srere (1999) *Intl Rev Cell & Mol Biol* 192.
- ¹⁰⁷ Ghosh SK, Cherstvy AG, Metzler R, work in progress.
- ¹⁰⁸ Strulson CA et al (2012) RNA catalysis through compartmentalization *Nature Chem* 4:941–946.
- ¹⁰⁹ Walter H, Brooks DE (1995) Phase separation in cytoplasm, due to macromolecular crowding, is the basis for microcompartmentation. *FEBS Lett* 361:135–139.
- ¹¹⁰ Dupuis NF, Holmstrom ED, Nesbitt DJ (2014) Molecular-crowding effects on single-molecule RNA folding/unfolding thermodynamics and kinetics. *Proc Natl Acad Sci USA* 111(23):8464–8469.
- ¹¹¹ Kang H, Pincus PA, Hyeon C, Thirumalai D (2014) Effects of macromolecular crowding on the collapse of biopolymers, arXiv:1409.5663
- ¹¹² Oh I, Choi S, Jung YJ, Kim JS (2014) Unusual size-dependence of effective interactions between collapsed polymers in crowded environments. *Soft Matter* 10:???–???. DOI: 10.1039/C4SM01486C.
- ¹¹³ Shendruk TN et al (2014) Simulating the Entropic Collapse of Coarse-Grained Chromosomes, arXiv:1407.2850.
- ¹¹⁴ In highly-crowded systems, which are the main targets of the current study, the polymer chain experiences collisions with many crowders around in the course of diffusion-limited looping. We thus believe hydrodynamic interactions to be of secondary importance for the static and dynamical effects considered here, likely just re-normalising the effective viscosity of the solution. As we demonstrate, rather the size of thermally-agitated crowders, which are to be displaced to ensure polymer looping, and their volume fraction are the dominant effects.
- ¹¹⁵ Note that starting from randomised chain configurations, in simulations of Ref.¹¹ the looping time was computed till the chain ends are closer than a ”critical” distance r_c . The latter is an important parameter that depends on the type of interactions which act between the chain ends. It has a meaning of effective inter-segmental distance at which e.g. DNA-protein-DNA contacts can be established, ≈ 3 -5 nm for a typical transcription factor.
- ¹¹⁶ Note that the one-dimensional end-monomer distribution function $p(r)$ does not involve a Jacobian to recover the free energy profile $F(r)$ since our end-to-end distance measurements already account for the spatial dilation.
- ¹¹⁷ The unlooping time is much shorter than the looping time and T_{ul} shows a weaker growth with n than T_l , compare

the two panels in Fig. 7. One possible reason is as follows. A looping event is the end-monomer encounter reaction that becomes progressively slower for larger polymer coils. The unlooping time in contrast is related to the (only moderately perturbed) diffusion of the polymer ends on the length-scale of the polymer coil, $r_{\text{eq}}(n) \sim R_g(n)$.

¹¹⁸ Such a statement is valid for *relatively weak* cohesion strength of the terminal monomers. In contrast, for very large end-to-end binding energies the unbinding kinetics is dominated by the dynamics of terminal monomers only, as illustrated by the Arrhenius-like behaviour for the unbinding events in Fig. 10 below. The motion of the polymer chain enables the accumulation of the energies $\gtrsim k_B T$ required to disrupt the bond between the polymer ends.

¹¹⁹ Note that Eq. (12) provides a satisfactory description of the looping times¹². Polymer looping is a prolonged barrier-crossing process in which the chain is close to equilibrium. For the reverse process of polymer unlooping, the disjoining of the end monomers takes place over a very short distance and spontaneous free-energy-downhill chain opening events occur (a process, which is inherently out of equilibrium). This is the main reason not to use the free energy-based Eq. (12) to evaluate the times of chain unlooping. The latter consists of two terms, the time of disjoining the end monomers and their diffusion from a close distance to the separation r_{eq} . Depending on the attraction strength ϵ_s , the relative contribution of the two terms to T_{ul} varies. For large ϵ_s values, for instance, the first contribution dominates so that the unlooping time exhibits the Arrhenius-like kinetics, see Eq. (14) and Fig. 10 below.

¹²⁰ The reason is as follows. The decay time characterising $\text{ACF}(\Delta)$ is related to the dynamics of *individual* monomer-crowder contacts. The interplay of these local fluctuations defines the life-time of a *cage* mediated by

larger crowders for the entire polymer. The looping time is, on the other hand, a target-search problem for the encounter reaction of the two polymer ends at the same small region of space. Being impeded by a topological polymer structure chain looping takes place typically on much longer time scales than T^* .

¹²¹ After submitting the current manuscript, we became aware of the recent studies of the crowder size^{111,112}. A stabilisation of intrinsically-disordered proteins and stabilisation of coil-to-globule transitions by crowding was discussed in Ref.¹¹¹, based on computer simulations of an MMC-induced compaction of polymers. It was shown e.g. that smaller crowders exerting a higher osmotic pressure onto the polymer compact it to a larger extent, as compared to the bigger ones. Contrary to our observations, particularly small crowders are excluded from the space occupied by the self-avoiding polymer. Similar to our results, Ref.¹¹¹ indicated that the size of the polymer coil reduces monotonically with ϕ . A slight non-monotonic $R_g(\phi)$ dependence obtained for the same system based on a phenomenological depletion potentials¹⁸ is thus rendered to be an artifact¹¹¹. The effects of MMC in our system are weaker than in Ref.¹¹¹ (we have the Flory-like scaling of polymer dimensions and no coil-to-globule transitions occur). The difference may be due to a smaller size of crowders in Ref.¹¹¹, as compared to the polymer monomers. Similarly to our results presented in Fig. 5b, in Ref.¹¹³ smaller crowders were shown to be more efficient in compacting the polymer chain. Lastly, in Ref.¹¹² the effects of the crowder size was investigated regarding the strength of depletion interactions between the *two* polymers. The strength of effective polymer-polymer attraction was shown to be reduced as the crowder size decreases (at a constant ϕ fraction).